Japanese Journal of Applied Physics **62**, SF1013 (2023) **REGULAR PAPER**
https://doi.org/10.35848/1347-4065/acbe04

Growth of α-Ga_2O_3 on α-Al_2O_3 by conventional molecular-beam epitaxy and metal–oxide-catalyzed epitaxy

J. P. McCandless[1*], D. Rowe[2], N. Pieczulewski[2], V. Protasenko[1], M. Alonso-Orts[3], M. S. Williams[3], M. Eickhoff[3], H. G. Xing[1,2,4], D. A. Muller[4,5], D. Jena[1,2,4], and P. Vogt[2,3]

[1]School of Electrical and Computer Engineering, Cornell University, Ithaca, New York, NY-14853, United States of America
[2]Department of Material Science and Engineering, Cornell University, Ithaca, New York, NY-14853, United States of America
[3]Institute of Solid-State Physics, University Bremen, Otto-Hahn-Allee 1, D-28359 Bremen, Germany
[4]Kavli Institute at Cornell for Nanoscale Science, Cornell University, Ithaca, New York, NY-14853, United States of America
[5]School of Applied and Engineering Physics, Cornell University, Ithaca, New York, NY-14853, United States of America

*E-mail: jpm432@cornell.edu

Received December 15, 2022; revised February 3, 2023; accepted February 22, 2023; published online March 23, 2023

We report the growth of α-Ga_2O_3 on *m*-plane α-Al_2O_3 by conventional plasma-assisted molecular-beam epitaxy and In-mediated metal–oxide-catalyzed epitaxy (MOCATAXY). We report a growth rate diagram for α-$Ga_2O_3(10\bar{1}0)$, and observe (i) a growth rate increase, (ii) an expanded growth window, and (iii) reduced out-of-lane mosaic spread when MOCATAXY is employed for the growth of α-Ga_2O_3. Through the use of In-mediated catalysis, growth rates over 0.2 μm h^{-1} and rocking curves with full width at half maxima of $\Delta\omega \approx 0.45°$ are achieved. Faceting is observed along the α-Ga_2O_3 film surface and explored through scanning transmission electron microscopy.

Supplementary material for this article is available online

1. Introduction

Over the past decade, Ga_2O_3 has gained much attention as a wide-band gap semiconductor. Monoclinic β-Ga_2O_3 possesses an ultra-wide bang gap of ~4.7 eV,[1] and it has been the most studied phase owing to its thermal stability and the availability of large-area, native, semi-insulating, and conductive substrates.[2,3] To further increase its band gap β-Ga_2O_3 can be alloyed with Al to form β-$(Al,Ga)_2O_3$, but achieving a high Al content has remained challenging due to the tendency to have phase segregation.[4] In contrast, α-$(Al,Ga)_2O_3$ becomes more stable as the Al is increased because the crystal is isostructural with the α-Al_2O_3 substrate and the lattice mismatch is reduced as the Al concentration is increased.[5] This has enabled the entire compositional range of α-$(Al,Ga)_2O_3$ to be readily achieved,[5,6] and it has enabled band gaps exceeding those of AlN, BN, or diamond.[7,8]

With the recent advances enabling α-Ga_2O_3 to remain stable during high-temperature anneals,[9] the next challenge is to achieve electrical conductivity. To date, conductivity in α-Ga_2O_3 has been achieved by chemical vapor deposition (CVD),[10,11] but has remained elusive for films grown by molecular-beam epitaxy (MBE). Additionally, conductive β-Ga_2O_3 films grown by MBE on α-Al_2O_3 have yet to be achieved.[7] While the exact reasons these films remain insulating are unknown, the thermodynamics during MBE growth and the low formation energy of defects may cause these Ga_2O_3 films on Al_2O_3 to be insulating.

Multiple compensating point defects (e.g. cation vacancies, oxygen vacancies, donor impurities[12,13]) and extended crystallographic defects (e.g. rotational domains and threading dislocations[14]) occur within the Ga_2O_3 films grown on sapphire. Reasons for the emergence of these defects include the lattice mismatch between the film and the substrate,[14] and the growth regime in which the films are grown.[12,13,15] For example, Ga vacancies (V_{Ga}) may act as compensating acceptors for introduced *n*-type dopants in grown Ga_2O_3 thin films.[15] O-rich growth environments are likely to generate a significant amount of V_{Ga} (due to their low formation energy) whereas Ga-rich growth environments are found to significantly suppress the formation of V_{Ga} (due to their high formation energy).[13] Thus, the growth of Ga_2O_3 in the highly Ga-rich regime—accessed by new epitaxial growth concepts[16,17]—may improve the transport properties of Ga_2O_3 thin films since the Ga-rich growth regimes lead to higher V_{Ga} formation energies, resulting in lower V_{Ga} densities within the Ga_2O_3 layers.

One approach to address these issues is through the use of metal–oxide-catalyzed epitaxy (MOCATAXY).[18] This is a growth process where a catalytic element (e.g. In) is introduced to the growth system and results in metal-exchange catalysis.[19] This growth mode has been observed for β-$(Al,Ga)_2O_3$ on different substrates and surface orientations, as well as for different epitaxial growth techniques.[20–24]

Many benefits arise from using MOCATAXY during the growth of Ga_2O_3. For example: (i) it can improve the surface morphologies of β-Ga_2O_3-based films.[21] (ii) The synthesis of Ga_2O_3 can occur in previously inaccessible kinetic and thermodynamic growth regimes (e.g. in highly metal-rich regimes) which can be beneficial for the suppression of undesired point (such as V_{Ga}) defects in Ga_2O_3.[12,13,19] (iii) The formation of thermodynamically unstable Ga_2O_3 phases becomes energetically favorable,[16,19,24] e.g. the formation of the ϵ/κ-phase of Ga_2O_3, which has enabled novel ϵ/κ-Ga_2O_3-based heterostructures.[23] (iv) The growth rate (Γ), possible growth temperatures (T_G), and crystalline quality of β-$(Al,Ga)_2O_3$-based thin films can be vastly enhanced.[18]

In this work, we introduce the growth of α-Ga_2O_3 by MOCATAXY, resulting in an expansion of the α-Ga_2O_3 growth window combined with an increased Γ and an improvement in its out-of-plane mosaic spread. It is the first demonstration of a catalytic growth process during the growth of α-Ga_2O_3.

2. Experimental

Samples were grown in a Veeco GEN930 plasma MBE system with standard Ga and In effusion cells. For all samples, the substrates were cleaned in acetone and isopropanol for 10 min and the α-Ga_2O_3 samples were grown for 60 min. The growth temperature (T_G) was measured by a thermocouple located within the substrate heater. The Ga flux (ϕ_{Ga}) and In flux (ϕ_{In}) were monitored by beam equivalent pressure (BEP) chamber readings. For conventional MBE and MOCATAXY, the O_2 flux (ϕ_O) was measured in standard cubic centimeters per min (SCCM) and a radio-frequency plasma power of 250 W was employed during all growths. To convert the measured values of ϕ_{Ga} (BEP), ϕ_{In} (BEP), and ϕ_O (SCCM) into units of $nm^{-2}\,s^{-1}$ conversion factors are taken from Ref. 25. Note, when using In-mediated catalysis, the available ϕ_O for Ga to Ga_2O_3 oxidation is about 2.8 times larger than for Ga oxidation in the absence of In.[16,19]

For samples grown by conventional MBE and MOCATAXY, the impact of ϕ_{Ga} and T_G is studied. In the case of MOCATAXY growth, the impact of ϕ_{In} is also investigated. All the growth parameters used in this work are collected in Table I. For scanning transmission electron microscopy (STEM), samples were prepared using a Thermo Fisher Helios G4 UX Focused Ion Beam with a final milling step of 5 keV to minimize damage. Carbon and Au–Pd layers were sputtered to reduce charging during sample preparation. Carbon and platinum protective layers were also deposited to minimize ion-beam damage. STEM measurements were taken with an aberration-corrected Thermo Fisher Spectra 300 CFEG operated at 300 keV.

3. Results and discussion

Figure 1 shows the growth-rate-diagram of α-$Ga_2O_3(10\bar{1}0)$ grown on α-$Al_2O_3(10\bar{1}0)$ by conventional MBE (the gray shaded area) and MOCATAXY (the purple shaded area). For conventionally grown samples two distinct growth regimes are observed: (i) the O-rich regime where O adsorbates are in excess over Ga adsorbates (i.e. the Ga flux limited regime), and (ii) the Γ-plateau regime (i.e. the Ga_2O desorption limited regime). The O-rich regime is characterized by an increasing Γ with increasing ϕ_{Ga}, whereas the plateau regime is characterized by a constant Γ, being independent of ϕ_{Ga}. Within this regime, however, Γ may decrease with increasing T_G (see inset in Fig. 1) as the desorption of the volatile suboxide Ga_2O becomes thermally more active.[26] The data in the inset of Fig. 1 plots Γ as a function of T_G for (i) α-Ga_2O_3 grown the O-rich regime and (ii) α-Ga_2O_3 grown in the Γ-plateau regime.

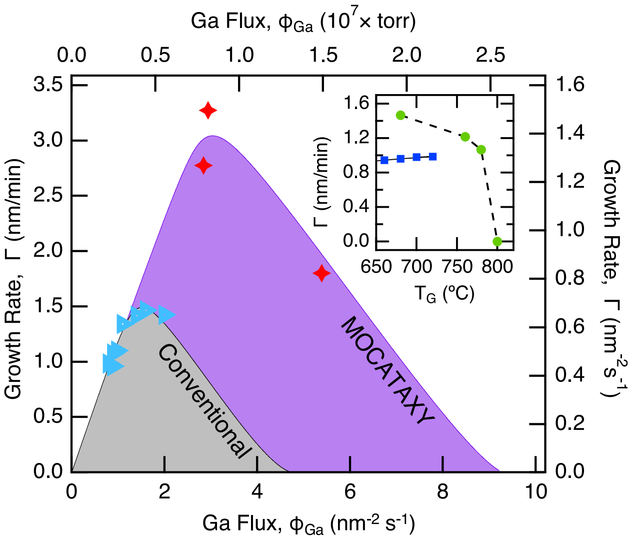

Fig. 1. (Color online) Growth-rate-diagram of α-$Ga_2O_3(10\bar{1}0)$ grown on α-$Al_2O_3(10\bar{1}0)$. The growth rate Γ as a function of ϕ_{Ga} at $T_G = 680$ °C is plotted for the growth by conventional MBE (blue triangles) and MOCATAXY (red stars). The Γ-data is fit by a Γ-model taken from Ref. 28. The gray shaded region shows the parameter space under which the formation of α-Ga_2O_3 by conventional MBE may occur. The purple shaded area depicts the growth regime of α-Ga_2O_3 assisted by MOCATAXY. Both fitted data sets were obtained at constant T_G and ϕ_O (values given in Table I). Inset: Γ as a function of T_G at two different fluxes of (i) $\phi_{Ga} = 0.9\ nm^{-2}\,s^{-1}$ (the O-rich regime, solid squares) and (ii) $\phi_{Ga} = 1.6\ nm^{-2}\,s^{-1}$ (the Γ-plateau regime, solid discs). A growth-rate-diagram of α-Ga_2O_3 as a function of ϕ_O is given in Ref. 27.

Table I. Collected growth parameters used in this work, values of ϕ_{Ga}, ϕ_{In}, ϕ_O, and T_G, for samples grown by conventional MBE and MOCATAX are listed. The conversion for ϕ_{Ga} and ϕ_{In} from BEP to nm min^{-1} to $nm^{-2}\,s^{-1}$ are $\phi_{Ga} = 2.5 \times 10^{-8}$ Torr $\hat{=}$ 1.1 nm min^{-1} $\hat{=}$ 1 $nm^{-2}\,s^{-1}$ and $\phi_{In} = 1.1 \times 10^{-7}$ Torr $\hat{=}$ 2.6 $nm^{-2}\,s^{-1}$, respectively.

Growth parameters	Conventional MBE	MOCATAXY
ϕ_{Ga} ($nm^{-2}\,s^{-1}$)	0.8–2.0	1.1–5.5
ϕ_{In} ($nm^{-2}\,s^{-1}$)	0	2.6–2.8
ϕ_O (SCCM)	1.4	0.7–1.0
ϕ_O ($nm^{-2}\,s^{-1}$)	2.2	3.2–4.6
T_G (°C)	640–800	680

To expand the accessible growth window of α-Ga_2O_3 to higher ϕ_{Ga} and to higher T_G, combined with increased Γ and improved crystalline quality, In-mediated catalysis was employed in the formation of α-Ga_2O_3.[19] The red stars in Fig. 1 show the resulting Γ as a function of ϕ_{Ga} at constant T_G. The gray shaded and purple shaded areas in Fig. 1 depict model-based descriptions of Γ for α-Ga_2O_3 grown by conventional MBE and MOCATAXY, respectively. The maximum Γ obtained for each growth technique is $\Gamma \approx 1.5$ nm min^{-1} and $\Gamma \approx 3.3$ nm min^{-1}, respectively. Using MOCATAXY, a more than 2-times increase in Γ for α-Ga_2O_3 at given growth conditions, as well as a shift far into the adsorption-controlled regime (i.e. far into the Ga-rich flux regime) is observed. This direct comparison between the two growth types clearly shows the expanded growth window made possible with MOCATAXY, for example, enabling $\Gamma \approx 1.8$ nm min^{-1} for α-Ga_2O_3 at $\phi_{Ga} = 5.5\ nm^{-2}\,s^{-1}$. In contrast, at these growth conditions, *no* growth of α-Ga_2O_3 is obtained by conventional MBE. The catalytic effect on Γ of α-Ga_2O_3 is modeled as a function of ϕ_O within the supplemental section.[27] We note that the depicted models use arbitrary kinetic parameters, based on kinetic parameters extracted for the growth ofβ-Ga_2O_3.[28]

To describe the growth of α-Ga_2O_3 by MOCATAXY, ϕ_O is scaled by a factor of 2.8 compared with the growth of α-Ga_2O_3 by conventional MBE. This additional O comes from the catalytic nature of In forming a catalytic adlayer (A) with O adsorbates, e.g. A= In–O, which provides more active O for the Ga to α-Ga_2O_3 oxidation. In other words, A increases the reaction probability of Ga with O on the respective growth surface, facilitating the formation of the final Ga_2O_3 compound at much higher ϕ_{Ga} and T_G, which enables excellent crystal quality.[16,19] We further note that the same factor of 2.8 was needed for modeling the MOCATAXY growth of β-Ga_2O_3 on different substrates and different surface orientations.[16,19] We note, however, that for a quantitative extraction of all kinetic growth parameters more Γ-studies of α-Ga_2O_3 are needed and are beyond the scope of this work. Nevertheless, the models help validate the Γ-data and provide insight into the growth regimes and growth mechanisms of α-Ga_2O_3. For example, once ϕ_{Ga} exceeds the active O flux, i.e. $\phi_{Ga} > \phi_O$, the growth will enter the Ga-rich regime and Γ will start to decrease, as shown by the gray shaded area in Fig. 1. Thus, this is the first direct indication that the growth of α-Ga_2O_3 is limited by the formation and subsequent desorption of Ga_2O, like what is observed for β-Ga_2O_3 grown by conventional MBE.[28]

Figure 2 directly compares the impact of both MBE growth techniques on the structural quality of the epitaxially grown films. In Fig. 2 (a), 2θ-ω XRD scans of two selected α-Ga_2O_3 films are shown, one grown by conventional MBE (depicted as the blue trace) and one grown by MOCATAXY (depicted as the red trace). The reflections of the films coincide with the α-Ga_2O_3 $30\bar{3}0$ peak. This, along with the absence of other diffraction peaks, indicates phase-pure α-$Ga_2O_3(10\,\bar{1}\,0)$ with In incorporation of $<1\%$ in the grown α-Ga_2O_3 layers, similar to what is observed for β-$(Al,Ga)_2O_3$ grown by MOCATAXY.[18] Figures 2(b) and 2(c) plot transverse scans (rocking curves) for the conventional MBE and MOCATXY grown α-Ga_2O_3 samples as plotted in Fig. 2(a). The rocking curves are measured across the symmetric $30\bar{3}0$ peak. The full width at half maxima (FWHM) of ω quantifies the out-of-plane mosaic spread of the α-Ga_2O_3 film. For conventionally grown films the out-of-plane crystal distribution is $\Delta\omega \approx 0.55°$ and for MOCATAXY grown films it is $\Delta\omega \approx 0.45°$. The film thicknesses d of the conventionally and MOCATAXY grown films are $d = 73$ nm and $d = 127$ nm, respectively. Jinno et al. reported that α-Ga_2O_3 films are fully relaxed for $d > 60$ nm.[5] Since lattice mismatch and relaxation are not impacted by MOCATAXY, it is noteworthy that despite the MOCATAXY film being thicker, $\Delta\omega$ is substantially smaller compared to what is obtained by conventional growth. The same MOCATAXY grown sample shown here is studied by STEM in Fig. 4.

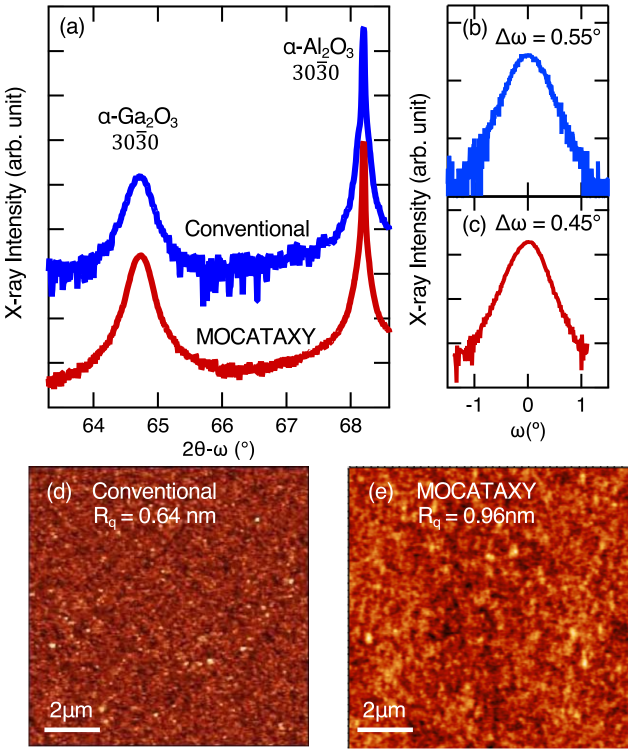

Fig. 2. (Color online) (a) Longitudinal XRD scans of optimized α-Ga_2O_3 films are shown. The reflections of the films coincide with the α-Ga_2O_3 $(10\bar{1}0)$ phase grown by conventional MBE (the blue trace) and MOCATAXY (the red trace). The used growth parameters were $\phi_{Ga} = 2.9\ \mathrm{nm^{-2}\,s^{-1}}$, $\phi_O = 1.4$ SCCM $\mathrel{\hat{=}}$ $2.2\ \mathrm{nm^{-2}\,s^{-1}}$, and $T_G = 750$ °C (conventional MBE), and $\phi_{Ga} = 2.9\ \mathrm{nm^{-2}\,s^{-1}}$, $\phi_{In} = 2.8\ \mathrm{nm^{-2}\,s^{-1}}$, $\phi_O = 0.7$ SCCM $\mathrel{\hat{=}} 3.2\ \mathrm{nm^{-2}\,s^{-1}}$, and $T_G = 680$ °C (MOCATAXY). (b) and (c) Transverse XRD scans across the $30\bar{3}0$ peak with their FWHM of $\Delta\omega = 0.55°$ (conventionally MBE-grown) and $\Delta\omega = 0.45°$ (MOCATAXY grown) are shown. These obtained $\Delta\omega$ are depicted in Fig. 3 at given ϕ_{Ga} and T_G. (d) and (e) Display surface morphologies obtained from $10 \times 10\ \mu$m AFM scans for α-$Ga_2O_3(10\bar{1}0)$ surfaces grown by conventional MBE and MOCATAXY, respectively. Growth conditions for the samples plotted in (d) and (e) are the same as for the ones plotted in panels (a)–(c), except a slightly lower $T_G = 730$ °C is used for the conventionally grown sample and a slightly higher supplied $\phi_O = 1.0$ SCCM for the MOCATAXY grown film. This resulted in $\Delta\omega = 0.61°$ and $\Gamma \approx 1.2\ \mathrm{nm\,min^{-1}}$ for the conventionally grown sample, and $\Delta\omega = 0.48°$ and $\Gamma > 3.0\ \mathrm{nm\,min^{-1}}$ for the MOCATAXY grown sample.

Surface morphologies and root mean square roughnesses (R_q) are measured by AFM and depicted in Figs. 2(d) and 2(e). The best surface roughness for conventionally grown α-Ga_2O_3 with $d = 66$ nm is $R_q = 0.64$ nm, while the smoothest one for MOCATAXY grown samples with $d \sim 270$ nm has an $R_q = 0.94$ nm. The larger surface roughness for the MOCATAXY grown sample is likely due to facetting on the top surface of the α-Ga_2O_3 thin film [see Fig. 4(a)]. We speculate that In does not only act as a catalyst but also acts as a surface active agent (surfactant) for the growth α-Ga_2O_3 thin films. It is widely understood that In can act as a surfactant for the epitaxial growth of GaN-based films,[29] and has also been observed during the growth of β-Ga_2O_3[21] and β-$(Al,Ga)_2O_3$.[18] Depending on the growth conditions and growth surface, which can affect the surface diffusion kinetics, surface chemical potentials, and the assessed growth mode, the suppression of facetting may be accomplished through the use of optimized conditions, while using In as a surfactant, enabling a modification in the surface free energies of the growing α-Ga_2O_3 thin film and a change in its growth mode.[18,21,30,31] However, surfactant-induced morphological phase-transitions from two-dimensional (2D) layer growth to three-dimensional (3D) island growth have also been observed during MBE growth.[32] We believe that a similar effect occurs for the α-Ga_2O_3 surfaces studied here when In may act as an (anti)surfactant during the growth of these films. Note, we have *not* fully explored all growth regimes made accessible through MOCATAXY in this study. Further studies may lead to additional improvements in the crystalline quality and surface morphologies of the α-Ga_2O_3 thin films.

In Figs. 3(a) and 3(b), the impact of ϕ_{Ga} and T_G, respectively, on $\Delta\omega$ for samples grown by conventional MBE in the O-rich regime (blue squares) and in the Γ-plateau regime (green circles), as well as for samples grown by

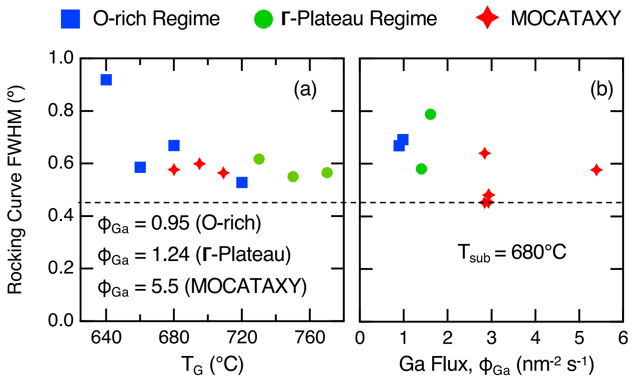

Fig. 3. (Color online) (a) and (b) FWHM (i.e. $\Delta\omega$ values) are plotted as a function of T_G and ϕ_{Ga}, respectively. Values are obtained by transverse XRD scans of the $30\bar{3}0$ peak of α-Ga_2O_3 grown films (XRD data not shown). Three distinct growth regimes are studied in panels (a) and (b): (i) the O-rich regime (blue squares), (ii) the Γ-plateau regime (green circles), and (iii) the MOCATAXY regime (red stars). The lowest value of $\Delta\omega$ is indicated by a dashed line. Note that for the samples grown by MOCATAXY, ϕ_{In} was varied between (2.6–2.8) $nm^{-2}\ s^{-1}$ and might explain the slight variations observed in $\Delta\omega$ for α-Ga_2O_3 grown at $\phi_{Ga} = 2.9\ nm^{-2}\ s^{-1}$ in panel (b)].

MOCATAXY (red stars), are shown. XRD data and $\Delta\omega$ are obtained by the same methods as described above for Fig. 2. Within the O-rich regime at $T_G = 640\ °C$, a large $\Delta\omega$ is observed, Fig. 3(a). At higher growth temperatures (i.e. $T_G \geqslant 660\ °C$), $\Delta\omega$ are similar (or slightly improving) with increasing temperature, regardless of growth regime. We speculate that the reason the crystal quality improves with T_G, is that there is an increase in the kinetic energy and a subsequent increase in the diffusion length of the adsorbates, allowing the Ga and O to reach the proper lattice site. However, if T_G is increased too much, a decrease in the surface lifetime of Ga adsorbates may occur, resulting in a reduction in the crystalline quality of the growing thin films. Using MOCATAXY in the Ga-rich regime with a fixed T_G, excess Ga may now reduce the needed surface diffusion length, improving the crystalline quality in the obtained α-Ga_2O_3 layers. More studies to separate the effects of ϕ_{Ga} and T_G on $\Delta\omega$ need to be performed, but to the best of our knowledge, the obtained $\Delta\omega$ values are the lowest reported in the literature for α-Ga_2O_3 grown on α-Al_2O_3.

Finally, to directly quantify and identify how MOCATAXY affects the crystal structure of α-Ga_2O_3 thin films, high-angle annular dark-field STEM (HAADF-STEM) was performed along the $\langle 0\bar{1}10\rangle$ zone axis, and is plotted in Fig. 4. The sample shown here is the same as the one shown in Fig. 2(c). In Fig. 4(a), a clear contrast differentiates the sapphire substrate, the epitaxial film (α-Ga_2O_3), and the protective Au–Pd sputtered coating. The bright contrast observed at the substrate/film interface (see Fig. 4(b) and Ref. 27) is due to additional scattering of the electron beam and indicates the presence of misfit dislocations. These dislocations arise due to the film relaxation caused by strain. A subset of the observed misfit dislocations propagate and lead to threading dislocations. From the contrast variation observed within the film [see Fig. 4(a)], an average frequency of one threading dislocation every 30 nm laterally along the film/substrate interface is observed. While more investigation is needed to determine the cause of the faceting and verify the above hypothesis (e.g. due to the changed growth mode when using In-mediated catalysis), it is observed that the threading dislocations can merge and then continue to propagate toward the film surface. These dislocations terminate at the bottom of intersecting surface planes, where faceting along the $(10\bar{1}1)$ plane is observed. The complimentary facet is unidentified since the facet is not perpendicular to the beam and tilts out-of-plane. This tilting is detected in Fig. 4(a) by the fading of contrast along the surface, in contrast to the sharp change in contrast on the $(10\bar{1}1)$ plane.

Figure 4(b) shows an enlarged image of the film/substrate interface. A pair of edge dislocations is observed and is highlighted with their Burgers circuits. This edge dislocation pair is observed along the film/substrate interface, and its dislocation density is estimated to be $5 \times 10^5\ cm^{-1}$ (or $\sim 10^{11}\ cm^{-2}$), i.e. occurring every 20 nm. This is similar to what is reported by conventional MBE.[5] To quantify Al/Ga inter-diffusion at the interface, a line scan (see S-Fig. 2 Ref. 27) was performed to quantify the contrast change. An interface width of $\sigma \approx 0.9$ nm was measured from an error

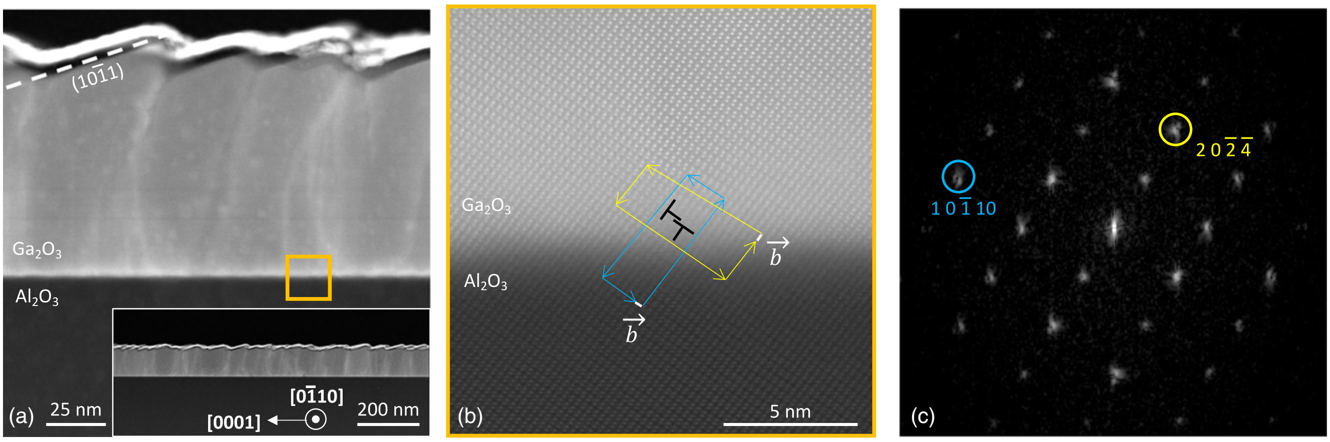

Fig. 4. (Color online) HAADF-STEM images show an overview of an α-$Ga_2O_3(10\bar{1}0)$ film grown on α-$Al_2O_3(10\bar{1}0)$. (a) The epitaxial film shows increased contrast due to misfit dislocations at the film/substrate interface. Threading dislocation propagate through the film and terminating at the intersection of its surface periodic faceting. (b) Enlarged image of the film-substrate interface (i.e. the α-Al_2O_3–α-Ga_2O_3 interface) is shown. Burger circuits are drawn around the edge dislocations. (c) Fast Fourier transform (FFT) of the interface region is shown. Diffraction peak separation at $(20\bar{2}\bar{4})$ and $(10\bar{1}10)$ indicate strain relaxation of the α-$Ga_2O_3(10\bar{1}0)$ on α-$Al_2O_3(10\bar{1}0)$.

function fitted to the Al intensity line scan profile (see S-Fig. 2 Ref. 27).

A fast Fourier transform (FFT), of the interface region shown in Fig. 4(b), is displayed in Fig. 4(c). A thin film completely strained to the substrate will show a singular diffraction peak. However, when the film relaxes its interplanar spacing d_{hkl} changes, resulting in an additional peak, shifted from the substrate peak. However, shifted peaks in the in-plane direction are not visible because the α-Ga_2O_3 $(000\bar{6})$ reflection peak is approximately 10x weaker than in α-Al_2O_3. The strain relaxation is observed in the $20\bar{2}\bar{4}$ and $10\bar{1}10$ diffraction peaks of α-Ga_2O_3. The strain relaxation is accomplished by the formation of edge dislocations at the interface, where the $20\bar{2}\bar{4}$ peak is correlated to the yellow Burgers circuit and the $10\bar{1}10$ peak to the cyan Burgers circuit. In addition, no phase separation or secondary phases were observed by STEM within the α-Ga_2O_3 film grown by MOCATAXY. However, a bi-layer structure from overlapping α-Ga_2O_3 grains when viewed in projection is observed with a slip along the $[10\bar{2}\bar{2}]$ direction (see S-Fig. 3 Ref. 27). The presence of this bi-layer structure indicates that the film is not single-crystalline. The bi-layer structure was confirmed using an ab initio TEM (*ab*TEM) simulation[33] which produced a matching HAADF image from the crystallographic information framework.

This TEM investigation of MOCATAXY grown α-Ga_2O_3 shows comparable crystal quality to what is measured for conventional MBE[5] with regards to edge dislocation density and phase purity. We note that the difference in projection direction may have prevented imaging of the bi-layer structure in this previous report. No faceting of α-Ga_2O_3 was observed by conventional MBE when grown on *m*-plane α-Al_2O_3.[5,9]

4. Conclusion

Phase-pure α-$Ga_2O_3(10\bar{1}0)$ on α-$Al_2O_3(10\bar{1}0)$ was grown using conventional MBE and MOCATAXY with thickness up to $d = 262$ nm. We mapped out the Γ-dependence on ϕ_{Ga} and T_{G} and its impact on the crystalline quality and surface morphologies. We identified and explored previously inaccessible growth regimes by MOCATAXY, and showed that it vastly extends the growth regime and improves the out-of-plane mosaic spread of the grown α-Ga_2O_3 films. Using In-mediated catalysis, we observe facetting on top of the α-$Ga_2O_3(10\bar{1}0)$ layers. This study confirms that this new MBE growth mode can be applied to the growth of α-Ga_2O_3–and is not limited to the growth of the β-Ga_2O_3 and β-$(Al,Ga)_2O_3$ polymorphs. We emphasize more studies are needed to determine the kinetic parameters that form α-Ga_2O_3 during conventional MBE and MOCATAXY growth, as well as to further improve the quality of the grown α-Ga_2O_3/α-Al_2O_3 heterostructures, and to understand the mechanisms leading to the surface faceting of α-Ga_2O_3.

Acknowledgments

This research is supported by the Air Force Research Laboratory-Cornell Center for Epitaxial Solutions (ACCESS), monitored by Dr. Ali Sayir (FA9550-18-1-0529). J. P. M. acknowledges the support of a National Science Foundation Graduate Research Fellowship under Grant No. DGE2139899. M. A.-O. acknowledges financial support from the Central Research Development Fund (CRDF) of the University of Bremen. This work makes use of PARADIM under Cooperative Agreement No. DMR-2039380. This work uses the CCMR and CESI Shared Facilities partly sponsored by the NSF MRSEC program (DMR-1719875) and MRI DMR-1338010, and the Kavli Institute at Cornell (KIC).

ORCID iDs

J. P. McCandless https://orcid.org/0000-0001-9084-7309
M. Alonso-Orts https://orcid.org/0000-0001-5043-4921
M. S. Williams https://orcid.org/0000-0003-3091-3890

1) H. H. Tippins, "Optical absorption and photoconductivity in the band edge of β-Ga_2O_3," Phys. Rev. **140**, A316 (1965).
2) Z. Galazka, R. Uecker, D. Klimm, K. Irmscher, M. Naumann, M. Pietsch, A. Kwasniewski, R. Bertram, S. Ganschow, and M. Bickermann, "Scaling-up of bulk β-Ga_2O_3 single crystals by the Czochralski method," ECS J. Solid State Sci. Technol. **6**, Q3007 (2017).
3) A. Kuramata, K. Koshi, S. Watanabe, Y. Yamaoka, T. Masui, and S. Yamakoshi, "High-quality β-Ga_2O_3 single crystals grown by edge-defined film-fed growth," Jpn. J. Appl. Phys. **55**, 1202A2 (2016).
4) A. F. U. Bhuiyan, Z. Feng, J. M. Johnson, H. L. Huang, J. Sarker, M. Zhu, M. R. Karim, B. Mazumder, J. Hwang, and H. Zhao, "Phase transformation in MOCVD growth of $(Al_xGa_{1-x})_2O_3$ thin films," APL Mater. **8**, 031104 (2020).
5) R. Jinno et al., "Crystal orientation dictated epitaxy of ultrawide-bandgap 5.4-to 8.6 eV $\alpha - (AlGa)_2O_3$ on *m*-plane sapphire," Sci. Adv. **7**, 1 (2021).
6) A. F. U. Bhuiyan, Z. Feng, H. L. Huang, L. Meng, J. Hwang, and H. Zhao, "Metalorganic chemical vapor deposition of α-Ga_2O_3 and α-Ga_2O_3 thin films on *m*-plane sapphire substrates," APL Mater. **9**, 101109 (2021).
7) M. Y. Tsai, O. Bierwagen, M. E. White, and J. S. Speck, "β-Ga_2O_3 growth by plasma-assisted molecular beam epitaxy," J. Vac. Sci. Technol. A **28**, 354 (2010).
8) G. Cassabois, P. Valvin, and B. Gil, "Hexagonal boron nitride is an indirect bandgap semiconductor," Nat. Photon. **10**, 262 (2016).
9) J. P. McCandless et al., "Thermal stability of epitaxial α-Ga_2O_3 and $(Al,Ga)_2O_3$ layers on *m*-plane sapphire," Appl. Phys. Lett. **119**, 062101 (2021).
10) K. Akaiwa and S. Fujita, "Electrical conductive corundum-structured α-Ga_2O_3 thin films on sapphire with tin-doping grown by spray-assisted mist chemical vapor deposition," Jpn. J. Appl. Phys. **51**, 070203 (2012).
11) T. Uchida, K. Kaneko, and S. Fujita, "Electrical characterization of Si-doped n-type α-Ga_2O_3 on sapphire substrates," MRS Adv. **3**, 171 (2018).
12) J. B. Varley, J. R. Weber, A. Janotti, and C. G. Van De Walle, "Oxygen vacancies and donor impurities in β-Ga_2O_3," Appl. Phys. Lett. **97**, 142106 (2010).
13) J. B. Varley, H. Peelaers, A. Janotti, and C. G. Van De Walle, "Hydrogenated cation vacancies in semiconducting oxides," J. Phys.: Condens. Matter **23**, 334212 (2011).
14) S. Rafique, L. Han, A. T. Neal, S. Mou, J. Boeckl, and H. Zhao, "Towards high-mobility heteroepitaxial β-Ga_2O_3 on sapphire-dependence on the substrate off-axis angle," Phys. Status Solidi A **215**, 1700467 (2018).
15) E. Korhonen, F. Tuomisto, D. Gogova, G. Wagner, M. Baldini, Z. Galazka, R. Schewski, and M. Albrecht, "Electrical compensation by Ga vacancies in Ga_2O_3 thin films," Appl. Phys. Lett. **106**, 242103 (2015).
16) P. Vogt, F. V. Hensling, K. Azizie, J. P. McCandless, J. Park, K. DeLello, D. A. Muller, H. G. Xing, D. Jena, and D. G. Schlom, "Extending the kinetic and thermodynamic limits of molecular-beam epitaxy utilizing suboxide sources or metal–oxide-catalyzed epitaxy," Phys. Rev. Appl. **17**, 034021 (2022).
17) P. Vogt et al., "Adsorption-controlled growth of Ga_2O_3 by suboxide molecular-beam epitaxy," APL Mater. **9**, 031101 (2021).
18) P. Vogt, A. Mauze, F. Wu, B. Bonef, and J. S. Speck, "Metal–oxide catalyzed epitaxy (MOCATAXY): the example of the O plasma-assisted molecular beam epitaxy of β-$(Al_xGa_{1-x})_2O_3$/β-Ga_2O_3 heterostructures," Appl. Phys. Express **11**, 115503 (2018).
19) P. Vogt, O. Brandt, H. Riechert, J. Lähnemann, and O. Bierwagen, "Metal-exchange catalysis in the growth of sesquioxides: towards heterostructures of transparent oxide semiconductors," Phys. Rev. Lett. **119**, 196001 (2017).
20) P. Mazzolini, P. Vogt, R. Schewski, C. Wouters, M. Albrecht, and O. Bierwagen, "Faceting and metal-exchange catalysis in (010) β-Ga_2O_3 thin films homoepitaxially grown by plasma-assisted molecular beam epitaxy," APL Mater. **7**, 022511 (2019).

21) A. Mauze, Y. Zhang, T. Itoh, F. Wu, and J. S. Speck, "Metal oxide catalyzed epitaxy (MOCATAXY) of β-Ga_2O_3 films in various orientations grown by plasma-assisted molecular beam epitaxy," APL Mater. **8**, 021104 (2020).

22) P. Mazzolini, A. Falkenstein, C. Wouters, R. Schewski, T. Markurt, Z. Galazka, M. Martin, M. Albrecht, and O. Bierwagen, "Substrate-orientation dependence of β-Ga_2O_3 (100), (010), (001), and ($\bar{2}$01) homo-epitaxy by indium-mediated metal-exchange catalyzed molecular beam epitaxy (MEXCAT-MBE)," APL Mater. **8**, 011107 (2020).

23) Y. Kuang et al., "Band alignment and enhanced interfacial conductivity manipulated by polarization in a surfactant-mediated grown κ-Ga_2O_3/In_2O_3 heterostructure," ACS Appl. Electron. Mater. **3**, 795 (2021).

24) M. Kracht et al., "Tin-assisted synthesis of ϵ-Ga_2O_3 by molecular beam epitaxy," Phys. Rev. Appl. **8**, 054002 (2017).

25) P. Vogt, "Growth kinetics, thermodynamics, and phase formation of group-iii and iv oxides during molecular beam epitaxy," PhD Thesis Humboldt University Berlin (2017).

26) P. Vogt and O. Bierwagen, "Reaction kinetics and growth window for plasma-assisted molecular beam epitaxy of Ga_2O_3: incorporation of Ga versus Ga_2O desorption," Appl. Phys. Lett. **108**, 072101 (2016).

27) See Supplemental Material for a model of Γ as a function of ϕ_O at $T_G = 680$ °C (S-Fig. 1) as well as images obtained by STEM (S-Figs. 2 and 3) and an included crystallographic model.

28) P. Vogt and O. Bierwagen, "Quantitative subcompound-mediated reaction model for the molecular beam epitaxy of III–VI and IV–VI thin films: applied to Ga_2O_3, In_2O_3, and SnO_2," Phys. Rev. Mater. **2**, 120401(R) (2018).

29) J. Neugebauer, T. K. Zywietz, M. Scheffler, J. E. Northrup, H. Chen, and R. M. Feenstra, "Adatom kinetics on and below the surface: the existence of a new diffusion channel," Phys. Rev. Lett. **90**, 056101 (2003).

30) M. Copel, M. Reuter, E. Kaxiras, and M. Tromp, "Surfactants in epitaxial growth," Phys. Rev. Lett. **63**, 632 (1989).

31) J. Neugebauer, "Surfactants and antisurfactants on group-III-nitride surfaces," Phys. Status Solidi C **0**, 1651 (2003).

32) R. B. Lewis, P. Corfdir, H. Li, J. Herranz, C. Pfuller, O. Brandt, and L. Geelhaar, "Quantum dot self-assembly driven by a surfactant-induced morphological instability," Phys. Rev. Lett. **119**, 086101 (2017).

33) J. Madsen and T. Susi, "The abTEM code: transmission electron microscopy from first principles," Open Res. Europe **1**, 13015 (2021).